



Published in final edited form as:

J Magn Reson Imaging. 2013 September ; 38(3): 751–756. doi:10.1002/jmri.24018.

Pulmonary Perfusion MRI using Interleaved Variable Density Sampling and Highly Constrained Cartesian Reconstruction (HYCR)

Kang Wang, Ph.D.^{1,2}, Mark L. Schiebler, M.D.³, Christopher J. Francois, M.D.³, A. Munoz Del Rio, Ph.D.^{2,3}, Ma. Daniela Cornejo, B.S.², Laura C. Bell, M.S.², Frank R. Korosec, Ph.D.^{2,3}, Jean H. Brittain, Ph.D.¹, James H. Holmes, Ph.D.¹, and Scott K. Nagle, Ph.D., M.D.^{2,3}

¹Global Applied Science Laboratory, GE Healthcare, Madison, WI

²Department of Medical Physics, University of Wisconsin-Madison, Madison, WI

³Department of Radiology, University of Wisconsin-Madison, Madison, WI

Abstract

Purpose—To demonstrate the feasibility of performing single breath-hold, non-cardiac gated, ultrafast, high spatial-temporal resolution whole chest MR pulmonary perfusion imaging in humans.

Materials and Methods—Eight (8) subjects (5 male, 3 female) were scanned with the proposed method on a 3T clinical scanner using a 32-channel phased-array coil. Seven (88%) were healthy volunteers, and one was a patient volunteer with sarcoidosis. The peak lung enhancement phase for each subject was scored for gravitational effect, peak parenchymal enhancement and severity of artifacts by 3 cardiothoracic radiologists independently.

Results—All studies were successfully performed by MR technologists without any additional training. Mean parenchymal signal was very good, measuring 0.78 ± 0.13 (continuous scale, 0 = “none” → 1 = “excellent”). Mean level of motion artifacts was low, measuring 0.13 ± 0.08 (continuous scale, 0 = “none” → 1 = “severe”).

Conclusion—It is feasible to perform single breath-hold, non-cardiac gated, ultrafast, high spatial-temporal resolution whole chest MR pulmonary perfusion imaging in humans.

Keywords

Pulmonary perfusion; IVD; HYCR; DCE MRI; constrained reconstruction; HYPR

INTRODUCTION

Assessment of pulmonary perfusion with dynamic contrast-enhanced (DCE) MRI is an important tool to help understand both the normal and abnormal physiology of the lung (1). Many diseases affect perfusion of the pulmonary vasculature and lung parenchyma itself, including acute and chronic pulmonary embolism (2), pulmonary hypertension (3,4), fibrotic lung disease (5), obstructive lung disease (6), cystic fibrosis (7) and congenital heart disease(8). Initial implementations of DCE for pulmonary perfusion MRI has been challenged by the need for complete 3D coverage of the lung with sufficient spatial

resolution. As Hopkins *et al.* suggested, an isotropic resolution better than 4.0 mm may not be necessary as this is the approximate size of the functional gas exchange unit in the lungs (9). More importantly, a high frame rate is necessary for the accurate assessment of pulmonary perfusion. For *qualitative* assessment of perfusion defects, the frame rate must be high enough to reliably capture the peak parenchymal signal throughout the 3D volume. For *quantitative* perfusion measurements, high frame rate is even more important because of the necessity for accurate measurement of the arterial input function (9). In previous works, a frame rate of 1.1 sec was used for quantitative assessment (2,3). Previous strategies for DCE pulmonary perfusion MRI have been reported, including use of an inversion recovery turbo flash sequence with short TE (10) and more recent work using non-Cartesian stack-of-stars *k*-space sampling with I-HYPR reconstruction (11). However, these techniques either lack sufficient spatial coverage along the slice encoding direction (10), or do not have the 4 mm isotropic spatial resolution (3,11) needed to assess the secondary lobule.

To obtain the desired frame rate without sacrificing spatial resolution, the MR data acquisition must be accelerated by reducing the number of measurements needed to reconstruct each time frame. Generally, *k*-space can be undersampled in two different ways. First, *k*-space can be undersampled **uniformly** (or “coherently”) during data acquisition and reconstructed using parallel imaging reconstruction methods (12–14). Alternatively, *k*-space can be undersampled **non-uniformly** (or “incoherently”), using Cartesian (15–18) or non-Cartesian (19,20) techniques. These non-uniform undersampling approaches can be combined with non-uniform temporal sampling rates and reconstructed using view-sharing reconstruction (15,16,21,22), model-based reconstruction (23–25), or constrained reconstruction methods such as HYPR (26–28) and compressed sensing (29). The view-sharing method uses all sampled *k*-space points in the time-frame being reconstructed, and approximates missing high frequency *k*-space by using data (either directly or through interpolation) acquired a short time before or after the current frame. Because of this, view-sharing can result in temporal blurring. To reduce this blurring, uniform and non-uniform sampling can be combined in the acquisition with view-sharing and parallel imaging applied sequentially in the reconstruction (15). Further, simulations using constrained reconstruction methods such as HYPR-like algorithms have suggested reduced temporal blurring from neighboring frames when compared to linear interpolation or nearest neighbor view-sharing (30,31). This may be important in depicting rapid changes in the contrast intensity curves and may be necessary for quantitation.

Recently, the combination of Interleaved Variable Density (IVD) sampling, **Highly** constrained **C**artesian **R**econstruction (HYCR), and parallel imaging has been used to achieve a very high acceleration factor ($\times 30$) when applied to DCE MR angiography of peripheral vascular disease (17). We have applied this IVD HYCR technique to 3D DCE pulmonary perfusion MRI, enabling the acquisition of perfusion images of the lungs with whole-chest coverage, high (1sec) frame rate and sufficient (4mm) isotropic spatial resolution in a single 20–25 sec breath-hold. The purpose of this work was to demonstrate the feasibility of using IVD HYCR to perform pulmonary perfusion MRI in humans.

MATERIALS AND METHODS

Imaging Protocol

Figure 1 shows the diagram for the imaging protocol. Eight (8) subjects (5 male, 3 female, average age 28y (19y–51y)) were scanned in this IRB-approved study. Seven (88%) were healthy volunteers, and one was a patient volunteer with sarcoidosis. All subjects were scanned on a 3T clinical scanner (Discovery MR750, GE Healthcare, Waukesha, WI, USA) using a 32-channel phased-array coil. This coil consists of an anterior and posterior part, with each part including 5 rows along S/I, and each row including 3 or 4 coil elements along

L/R. Scan parameters included: sagittal excitation slab, full chest coverage, TR/TE = 1.8/0.5 ms, 75% fractional echo, BW = ± 125 kHz, matrix = 100 (S/I) \times $(56-70)$ (A/P) \times 100 (L/R), FOV = 40 (S/I) \times $(23-28)$ (A/P) \times 40 (L/R) cm³, parallel imaging factor = 2×2 , IVD factor = 3 , yielding a total acceleration factor of approximately 12 . This enabled whole-chest coverage with 4.0 mm isotropic spatial resolution and frame rate of 1.0 sec/volume. The healthy subjects received $0.5 \times$ dose (0.015 mmol/kg) of gadofosveset trisodium (Lantheus Medical Imaging, North Billerica, MA, USA) while the sarcoidosis patient received a $0.5 \times$ dose (0.05 mmol/kg) of gadobenate dimethylglumine (Bracco Diagnostics, Princeton, NJ, USA) as part of a routine clinical cardiac MRI study, injected through a $20G$ antecubital intravenous catheter. The duration of the contrast injection in all subjects was 2 sec, followed by a $15-30$ mL saline bolus injected at the same rate. A pre-contrast mask was acquired during the first $3-4$ seconds following injection, before contrast reached the superior vena cava or heart. Sixteen (16) to eighteen (18) volumes were then acquired at 1.0 sec/volume during an end-expiration single total breath-hold of $20-25$ sec (including the mask).

Image Reconstruction

Images were reconstructed using Highly constrained Cartesian Reconstruction (HYCR) combined with ARC, a coil-by-coil data-driven parallel imaging reconstruction described as Method 5 in Ref. (14), with a 3D kernel size of 3 (frequency) \times 7 (phase) \times 7 (slice). Briefly, after complex mask subtraction of the data in k -space, three intermediate images were generated. First, the data from each time frame (i.e. 1.0 second duration in this application) are reconstructed using zero-filling and parallel imaging, producing an image, I_b , with some spatial blurring artifacts but minimal temporal blurring relative to the composite image described below. Second, data from a sliding window with a 7 sec temporal footprint are summed to eliminate IVD undersampling and then density corrected to reconstruct a composite image I_t that is temporally blurred but has minimal spatial artifacts compared to image I_b . Then, the image I_t is sub-sampled at the same k -space locations as measured for I_b and reconstructed using zero-filling and parallel imaging. The resulting image \tilde{I}_t serves as a normalization factor. The final high frame rate and high spatial resolution HYCR image is then calculated as

$$\hat{I}_t = \tilde{I}_t \cdot \frac{I_t + c}{\tilde{I}_t + c}, \quad [1]$$

where c is a small regularization constant to avoid zero division. This algorithm is described in detail in Ref. (17). The diagram for image reconstruction is also included in Figure 1.

Imaging Analysis

The 3D volumes corresponding with peak lung enhancement from each scan, obtained by reviewing the coronal maximum intensity projection (MIP) time frame images, were randomized and independently scored by 3 cardiothoracic radiologists. As a surrogate measure of parenchymal enhancement, the ability to identify the normal increase in perfusion in the dependent portions of the lungs (gravitational effect) was scored using a 3-point scale (0 = “not seen”, 1 = “present”, 2 = “well seen”). Peak parenchymal enhancement and severity of artifacts were graded on continuous scales: 0 (none) \rightarrow 1 (excellent) for enhancement and 0 (none) \rightarrow 1 (severe) for artifacts. Paired two-tailed t-tests were used to compare the readers’ individual scores. P-values of < 0.05 were considered significant. The average scores across readers were then used to calculate summary statistics of parenchymal enhancement and artifact severity across the 8 cases, reported as mean \pm 95% confidence interval.

To estimate perfusion maps, the following equations (32) were used on a voxel-by-voxel basis. The relative pulmonary blood volume (rPBV) was estimated as area under the curve, *i.e.*

$$rPBV = \int S(t) \cdot dt \quad [2]$$

The Mean Transit Time (MTT) was estimated as the first moment normalized by the rPBV, *i.e.*

$$MTT = \frac{\int S(t) \cdot t \cdot dt}{\int S(t) \cdot dt} \quad [3]$$

The relative pulmonary blood flow (rPBF) was estimated as the relative ratio between rPBV and MTT, *i.e.*

$$rPBF = \frac{rPBV}{MTT} \quad [4]$$

Please note that the equations above do not represent the true quantification as deconvolution of the arterial input function was not performed.

RESULTS

The scans were successfully completed in all subjects. Figure 2 shows the results from a typical healthy volunteer. Figure 2(a) shows coronal maximum intensity projection (MIP) images at 9 consecutive time frames. From this time series, the peak lung enhancement can be identified (in this case at time $t = 15s$), and the entire 3D volume at this time point can be visualized in any orientation with 4.0 mm isotropic resolution, as shown in Figure 2(b). Note that the locations of the major fissures can be seen in the coronal and axial views (top and middle image in Figure 2(b)) as relatively low intensity lines, reflecting the amount of enhancement present in the lung tissue itself. Figure 2(c) shows measured temporal waveforms and estimated perfusion maps. Figure 3 shows images from the clinical patient with stage III sarcoidosis. The peak lung enhancement phase images show both the isotropic resolution and full chest coverage of the technique. Large perfusion defects (white arrows) correlate with areas of extensive fibrosis seen on CT (black arrows). The perfusion maps for the same axial slice are included in Figure 3(e–g) and also show the defects.

Table 1 shows the image quality scores recorded for all readers and subjects. Mean parenchymal signal was very good, measuring 0.78 ± 0.13 . Mean level of motion artifacts was low, measuring 0.13 ± 0.08 . Paired two-tailed t-tests demonstrated no statistically significant difference in the scores between the 3 readers ($p = 1.00, 0.17, 0.45$ for gravitational effect; $p = 0.70, 0.84, 0.60$ for parenchymal enhancement; and $p = 0.61, 0.16,$ and $p=0.71$ for motion artifact).

DISCUSSION

This work demonstrates the feasibility of obtaining 3D pulmonary perfusion MR images of the whole-chest with a high frame rate (1.0 sec) and isotropic 4mm spatial resolution, using IVD HYCR (17). Prior work has suggested that pulmonary perfusion varies only down to the size of the functional gas exchange unit, which is thought to be roughly 90 mm^3 (~4.5 mm isotropic resolution) (9), and that further improvement in spatial resolution may not

yield any additional information. However the true answer to this question remains unknown. Generally, this single breath-hold protocol is not dependent on bolus timing – no test bolus or real-time trigger is needed – and may be incorporated into routine clinical scan without additional training of MR technologists.

Several features of IVD HYCR contribute to its suitability to pulmonary perfusion MRI. First, a sagittal excitation is used in order to avoid aliasing from the arms. Second, even though there is very little baseline signal in the lungs prior to contrast administration, a pre-contrast mask is acquired at the start of the scan, before contrast reaches the superior vena cava or the heart. This allows the use of subtraction to suppress the high signal from subcutaneous fat. Finally, because the T_2^* in the lungs is very short (~2 ms) (33), a high bandwidth (± 125 kHz) and a fractional echo (75%) is used to minimize the TE (0.5ms).

Respiratory and cardiac motion can be major sources of artifact in pulmonary perfusion MRI. Respiratory motion artifacts usually manifest as residual bright signal arising from the subcutaneous fat due to mis-registration between the mask and dynamic time frame data. The breath-hold time of this protocol is 20–25 sec, which is well tolerated by most patients. However, this may cause difficulties when imaging dyspneic patients, such as patients with significant chronic obstructive pulmonary disease (COPD) or advanced pulmonary hypertension. In cases in which a patient breathes before the end of the scan, the peak parenchymal enhancement phase will typically be captured between $t = 13\text{--}18$ sec post injection, before the breathing occurs, providing useful qualitative diagnostic information. Some cardiac motion artifacts were observed; however, these artifacts only affected the heart itself and did not limit the visualization of the lungs (34).

This work uses a small number of subjects to demonstrate the technical feasibility of performing single breath-hold pulmonary perfusion with high spatial-temporal resolution in clinical setting. A limitation of this work is that the analysis of perfusion in this study was qualitative or semi-quantitative assessment. Future work will involve a larger number of both healthy subjects and patients with lung pathology, and will include the identification of the arterial input function (AIF) and a deconvolution algorithm to calculate quantitative pulmonary perfusion parameter maps, such as the PBV, MTT and PBF. With such true quantitative analysis, comparison of various acquisition and reconstruction methods could be performed to evaluate the relative advantages and disadvantages of the alternative techniques, including the HYCR method used in this study.

In this work, we have demonstrated the feasibility of using IVD HYCR to obtain 3D pulmonary perfusion MR images of the whole-chest with a high frame rate (1.0 sec/frame) and good isotropic spatial resolution (4.0 mm) in humans. The entire scan is clinically practical, as it only requires a single 20–25 second breath-hold and does not require either bolus-timing or cardiac or respiratory gating.

Acknowledgments

The authors would like to thank Dr. Jiang Du for his help on this project. We would also like to extend our appreciation to Sara Pladziewicz and Kelli Hellenbrand for recruiting and scanning the subjects. The authors also gratefully acknowledge the support of the Department of Radiology Research and Development Committee.

Grant sponsor: UW Radiology R&D Committee; NIH

Grant numbers: NIH-R01 EB006882;

REFERENCES

1. Hatabu H, Tadamura E, Levin DL, et al. Quantitative assessment of pulmonary perfusion with dynamic contrast-enhanced MRI. *Magn Reson Med.* 1999; 42:1033–1038. [PubMed: 10571924]
2. Ohno Y, Koyama H, Matsumoto K, et al. Dynamic MR perfusion imaging: capability for quantitative assessment of disease extent and prediction of outcome for patients with acute pulmonary thromboembolism. *J Magn Reson Imaging.* 2010; 31:1081–1090. [PubMed: 20432342]
3. Ohno Y, Hatabu H, Murase K, et al. Quantitative assessment of regional pulmonary perfusion in the entire lung using three-dimensional ultrafast dynamic contrast-enhanced magnetic resonance imaging: Preliminary experience in 40 subjects. *J Magn Reson Imaging.* 2004; 20:353–365. [PubMed: 15332240]
4. Ley S, Grunig E, Kiely DG, van Beek E, Wild J. Computed tomography and magnetic resonance imaging of pulmonary hypertension: Pulmonary vessels and right ventricle. *J Magn Reson Imaging.* 2010; 32:1313–1324. [PubMed: 21105137]
5. Yi CA, Lee KS, Han J, Chung MP, Chung MJ, Shin KM. 3-T MRI for differentiating inflammation- and fibrosis-predominant lesions of usual and nonspecific interstitial pneumonia: comparison study with pathologic correlation. *AJR Am J Roentgenol.* 2008; 190:878–885. [PubMed: 18356432]
6. Ley-Zaporozhan J, Ley S, Kauczor HU. Morphological and functional imaging in COPD with CT and MRI: present and future. *Eur Radiol.* 2008; 18:510–521. [PubMed: 17899100]
7. Eichinger M, Puderbach M, Fink C, et al. Contrast-enhanced 3D MRI of lung perfusion in children with cystic fibrosis--initial results. *Eur Radiol.* 2006; 16:2147–2152. [PubMed: 16673092]
8. Sridharan S, Derrick G, Deanfield J, Taylor AM. Assessment of differential branch pulmonary blood flow: a comparative study of phase contrast magnetic resonance imaging and radionuclide lung perfusion imaging. *Heart.* 2006; 92:963–968. [PubMed: 16775104]
9. Hopkins SR, Prisk GK. Lung perfusion measured using magnetic resonance imaging: New tools for physiological insights into the pulmonary circulation. *J Magn Reson Imaging.* 2010; 32:1287–1301. [PubMed: 21105135]
10. Hatabu H, Gaa J, Kim D, Li W, Prasad PV, Edelman RR. Pulmonary perfusion: qualitative assessment with dynamic contrast-enhanced MRI using ultra-short TE and inversion recovery turbo FLASH. *Magn Reson Med.* 1996; 36:503–508. [PubMed: 8892200]
11. Artz, NS.; O'Halloran, RL.; Schiebler, M.; Holmes, JH.; Fain, SB. Dynamic Contrast Enhanced Pulmonary Perfusion with Undersampled Stack-of-Stars and Iterative Highly Constrained Back-Projection. *Proc 18th Annual Meeting ISMRM; Stockholm, Sweden.* 2010. p. 4622
12. Pruessmann KP, Weiger M, Scheidegger MB, Boesiger P. SENSE: sensitivity encoding for fast MRI. *Magn Reson Med.* 1999; 42:952–962. [PubMed: 10542355]
13. Griswold MA, Jakob PM, Heidemann RM, et al. Generalized autocalibrating partially parallel acquisitions (GRAPPA). *Magn Reson Med.* 2002; 47:1202–1210. [PubMed: 12111967]
14. Brau AC, Beatty PJ, Skare S, Bammer R. Comparison of reconstruction accuracy and efficiency among autocalibrating data-driven parallel imaging methods. *Magn Reson Med.* 2008; 59:382–395. [PubMed: 18228603]
15. Haider CR, Hu HH, Campeau NG, Huston J 3rd, Riederer SJ. 3D high temporal and spatial resolution contrast-enhanced MR angiography of the whole brain. *Magn Reson Med.* 2008; 60:749–760. [PubMed: 18727101]
16. Du J. Contrast-enhanced MR angiography using time resolved interleaved projection sampling with three-dimensional cartesian phase and slice encoding (TRIPPS). *Magn Reson Med.* 2009; 61:918–924. [PubMed: 19195019]
17. Wang K, Busse RF, Holmes JH, et al. Interleaved variable density sampling with a constrained parallel imaging reconstruction for dynamic contrast-enhanced MR angiography. *Magn Reson Med.* 2011; 66:428–436. [PubMed: 21360740]
18. Korosec FR, Frayne R, Grist TM, Mistretta CA. Time-resolved contrast-enhanced 3D MR angiography. *Magn Reson Med.* 1996; 36:345–351. [PubMed: 8875403]
19. Peters DC, Korosec FR, Grist TM, et al. Undersampled projection reconstruction applied to MR angiography. *Magn Reson Med.* 2000; 43:91–101. [PubMed: 10642735]

20. Meyer CH, Hu BS, Nishimura DG, Macovski A. Fast spiral coronary artery imaging. *Magn Reson Med.* 1992; 28:202–213. [PubMed: 1461123]
21. Du J, Carroll TJ, Brodsky E, et al. Contrast-enhanced peripheral magnetic resonance angiography using time-resolved vastly undersampled isotropic projection reconstruction. *J Magn Reson Imaging.* 2004; 20:894–900. [PubMed: 15503332]
22. Mostardi PM, Haider CR, Rossman PJ, Borisch EA, Riederer SJ. Controlled experimental study depicting moving objects in view-shared time-resolved 3D MRA. *Magn Reson Med.* 2009; 62:85–95. [PubMed: 19319897]
23. Chandra S, Liang ZP, Webb A, Lee H, Morris HD, Lauterbur PC. Application of reduced-encoding imaging with generalized-series reconstruction (RIGR) in dynamic MR imaging. *J Magn Reson Imaging.* 1996; 6:783–797. [PubMed: 8890017]
24. Tsao J, Boesiger P, Pruessmann KP. k-t BLAST and k-t SENSE: dynamic MRI with high frame rate exploiting spatiotemporal correlations. *Magn Reson Med.* 2003; 50:1031–1042. [PubMed: 14587014]
25. Jung H, Sung K, Nayak KS, Kim EY, Ye JC. k-t FOCUSS: a general compressed sensing framework for high resolution dynamic MRI. *Magn Reson Med.* 2009; 61:103–116. [PubMed: 19097216]
26. Mistretta CA, Wieben O, Velikina J, et al. Highly constrained backprojection for time-resolved MRI. *Magn Reson Med.* 2006; 55:30–40. [PubMed: 16342275]
27. Johnson KM, Velikina J, Wu Y, Kecskemeti S, Wieben O, Mistretta CA. Improved waveform fidelity using local HYPR reconstruction (HYPR LR). *Magn Reson Med.* 2008; 59:456–462. [PubMed: 18306397]
28. Huang Y, Wright GA. Time-resolved MR angiography with limited projections. *Magn Reson Med.* 2007; 58:316–325. [PubMed: 17654575]
29. Lustig M, Donoho D, Pauly JM. Sparse MRI: The application of compressed sensing for rapid MR imaging. *Magn Reson Med.* 2007; 58:1182–1195. [PubMed: 17969013]
30. Keith L, Kecskemeti S, Velikina J, Mistretta C. Simulation of relative temporal resolution of time-resolved MRA sequences. *Magn Reson Med.* 2008; 60:398–404. [PubMed: 18666099]
31. Busse, RF.; Pineda, AR.; Wang, K.; Holmes, JH.; Brittain, JH.; Korosec, FR. Time-Resolved Imaging with Multiplicative Algebraic Reconstruction Technique (MART): An Application of HYPR Principles for Variable Density Cartesian Acquisitions. *Proc 17th Annual Meeting ISMRM; Hawai'i, USA.* 2009. p. 2834
32. Meier P, Zierler KL. On the theory of the indicator-dilution method for measurement of blood flow and volume. *J Appl Physiol.* 1954; 6:731–744. [PubMed: 13174454]
33. Hatabu H, Alsop DC, Listerud J, Bonnet M, Gefter WB. T2* and proton density measurement of normal human lung parenchyma using submillisecond echo time gradient echo magnetic resonance imaging. *Eur J Radiol.* 1999; 29:245–252. [PubMed: 10399610]
34. Wang, K.; Schiebler, M.; Francois, C., et al. Utility of Cardiac Gating for Pulmonary Perfusion MRI. *Proc 19th Annual Meeting ISMRM; Montreal, Canada.* 2011. p. 1526

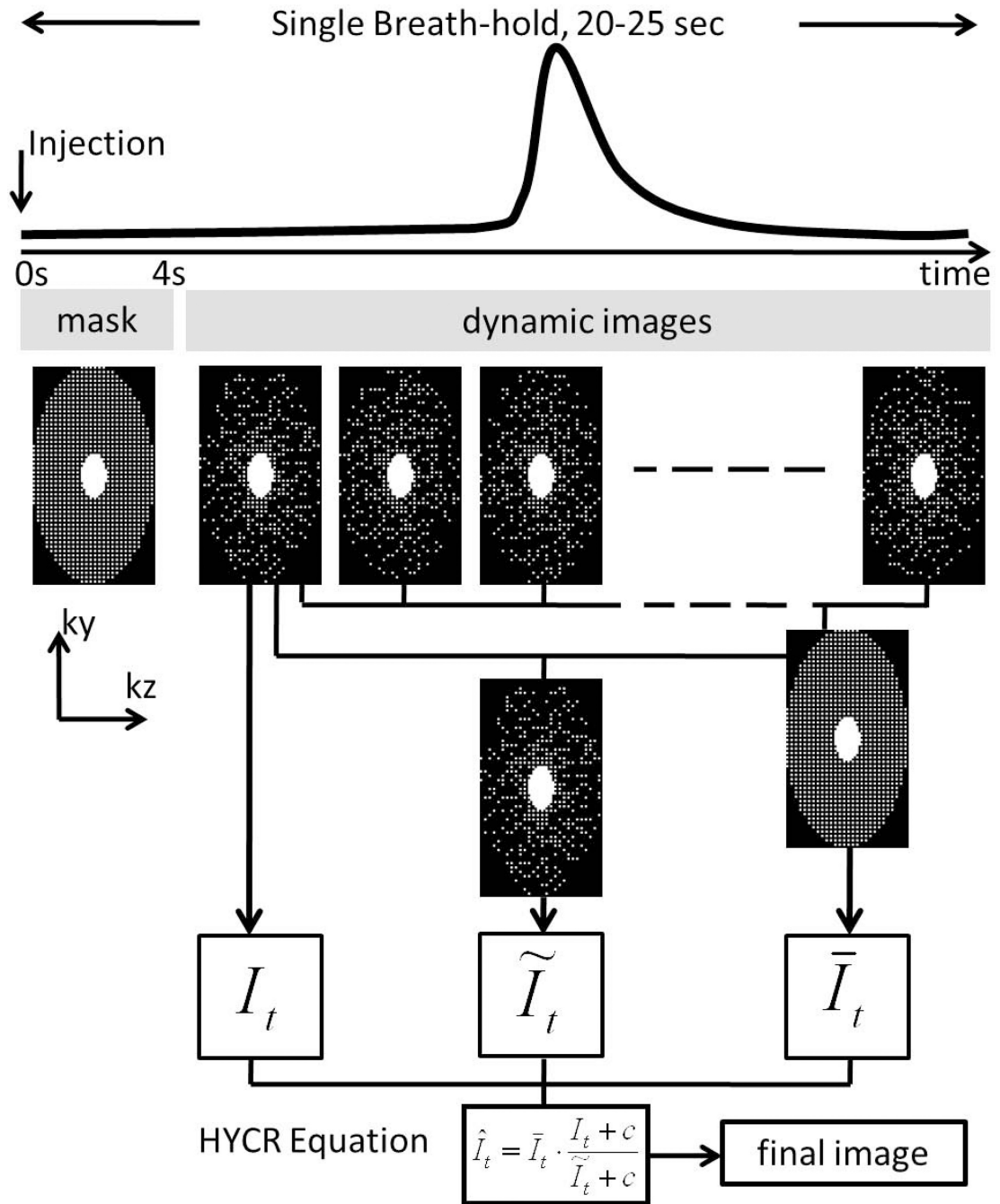


Figure 1.

Imaging protocol and reconstruction diagram. The injection and the acquisition are started at the same time. A mask data set is acquired before the contrast arrival, followed immediately by the dynamic acquisition of approximately 18 time frames. In reconstruction, a k -space mask subtraction is performed (not shown in the diagram) before the dynamic k -space data are sent to HYCR reconstruction. Please refer to the Theory section and Ref. (17) for more reconstruction details.

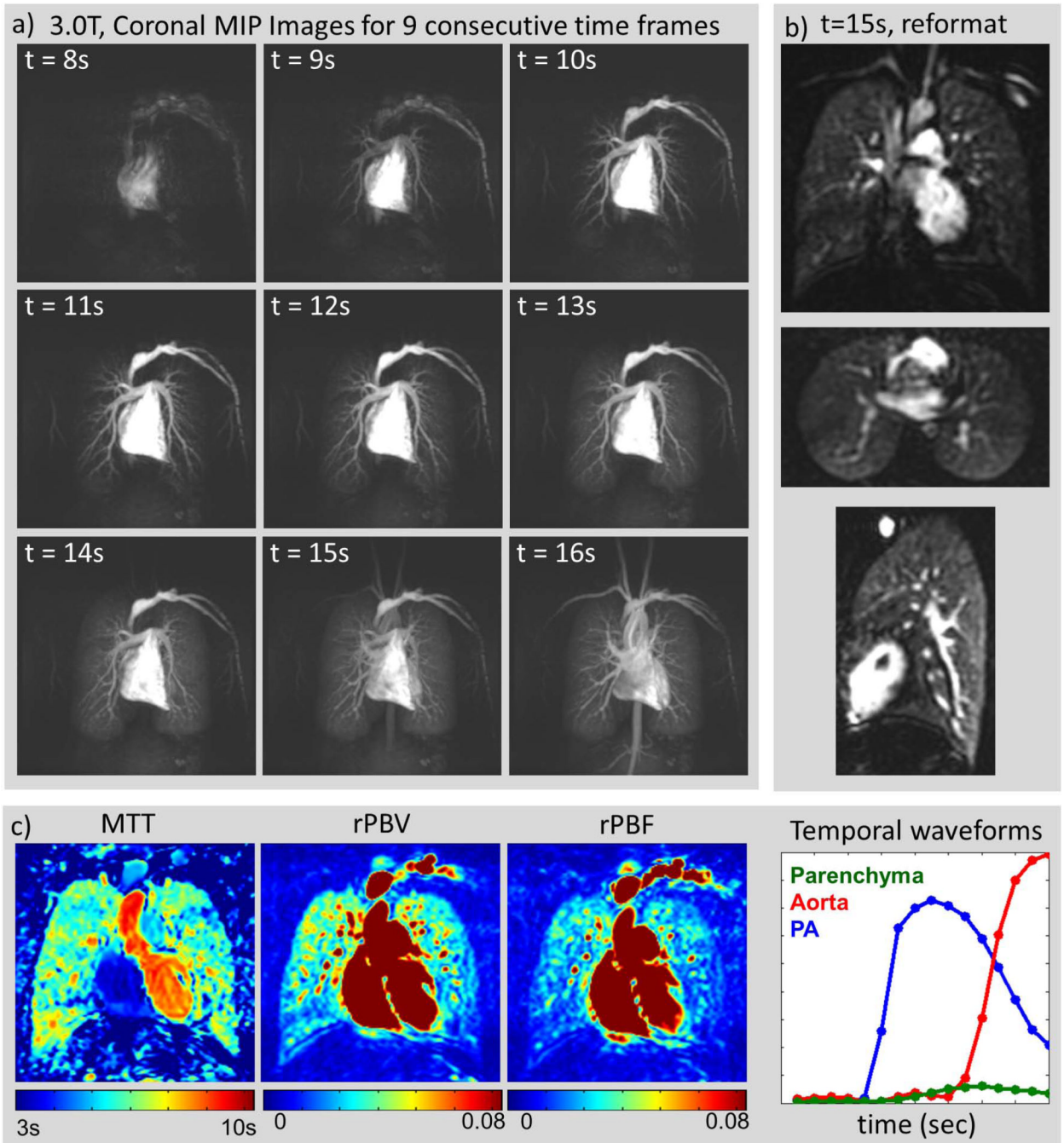


Figure 2.

Healthy Volunteer. (a): Consecutive coronal maximum intensity projection (MIP) images from a healthy volunteer scanned at 3.0T with a 32-channel torso receiver array, $40(S/I) \times 40(L/R) \times 24(A/P)$ cm³ whole-chest coverage, 4.0mm isotropic spatial resolution, and 1.0 sec/frame. Times are from the start of the injection. The entire passage of the bolus is well depicted. (b): The entire lung at the peak parenchyma enhancement point (here t=15s) can be visualized in coronal (top), axial (middle) and sagittal (bottom) views due to the isotropic resolution. Note that the fissures are visible in the coronal and axial views, indicative of the amount of parenchymal enhancement observed. (c) Estimated perfusion maps and temporal waveforms for selected regions of interest: parenchyma, aorta and pulmonary artery (PA).

3.0T, sarcoidosis case

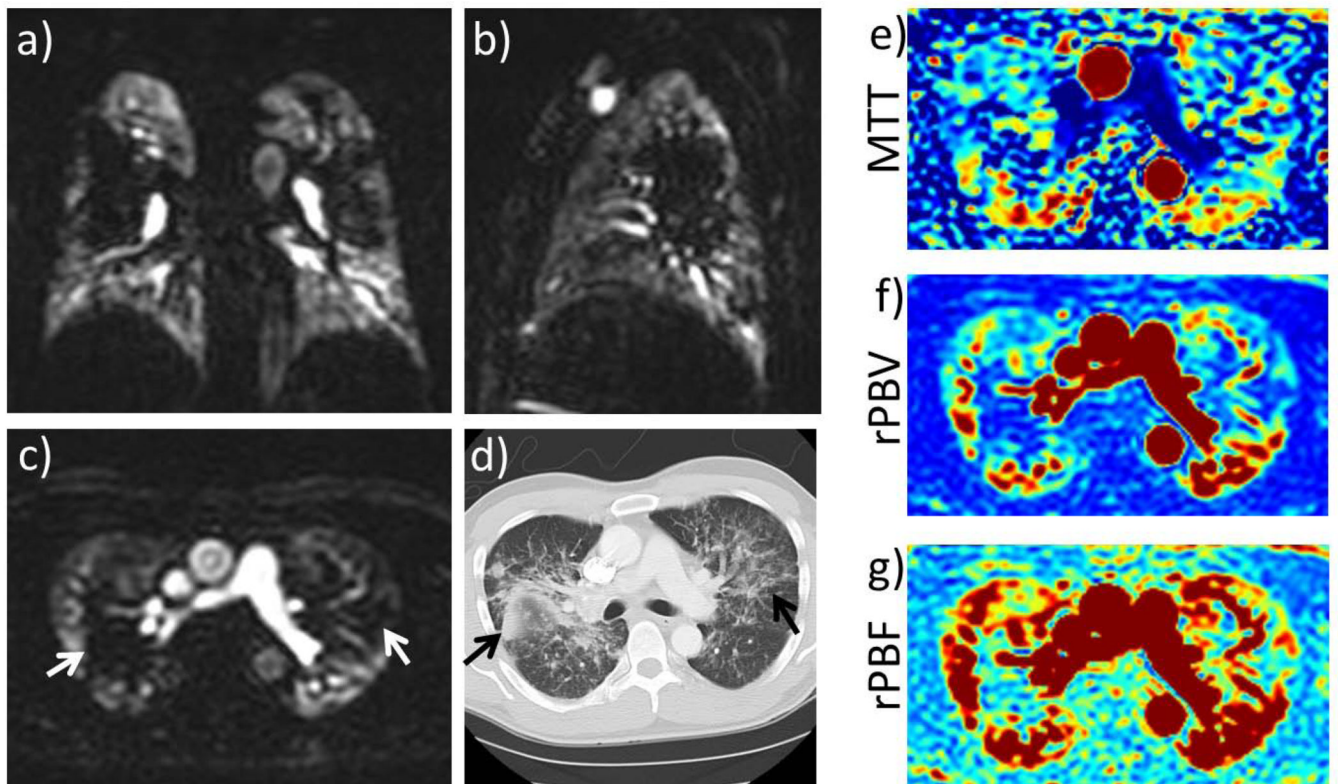
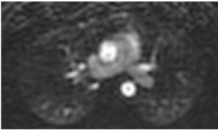






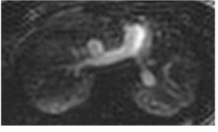
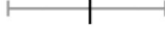
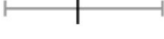




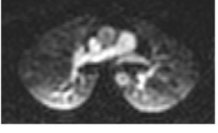






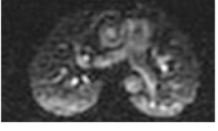






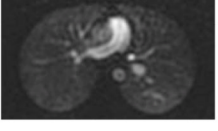






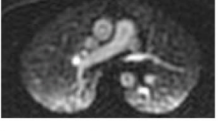






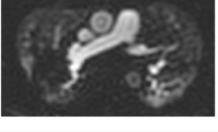






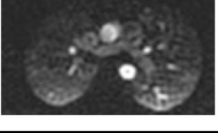








Figure 3. Patient volunteer with sarcoidosis. Representative slices in (a) coronal, (b) sagittal and (c) axial views at the peak parenchymal enhancement phase. Large perfusion defects in the central regions of both lungs (white arrows), corresponding to (d) the areas of fibrosis seen on CT (black arrows). The perfusion maps (e–g) for the same axial slice also show the defects.

Table 1

Scoring results for all cases

Case	Parenchymal Signal	Motion Artifacts
1 	 0.44	 0.23
	 0.56	 0.37
	 0.71	 0.06
2 	 0.52	 0.46
	 0.38	 0.17
	 0.37	 0.51
3 	 0.92	 0.05
	 0.79	 0.13
	 0.86	 0.06
4 	 0.87	 0.24
	 0.87	 0.06
	 0.90	 0.06
5 	 0.95	 0.08
	 0.95	 0.06
	 0.95	 0.02
6 	 0.94	 0.05
	 0.95	 0.10
	 0.78	 0.05
7 	 0.84	 0.05
	 0.87	 0.05
	 0.79	 0.08
8 	 0.73	 0.11
	 0.75	 0.13
	 0.95	 0.03

Parenchymal signal (0 = “none” → 1 = “excellent”) and motion artifacts (0 = “none” → 1 = “severe”). A representative axial slice was shown in the first column for each subject. Subject 7 was a patient volunteer with sarcoidosis. The other subjects were healthy volunteers.